MODEL-BASED ESTIMATION OF T2 MAPS WITH DUAL-ECHO STEADY-STATE MR IMAGING

Gopal Nataraj[⋆] *Jon-Fredrik Nielsen*[†] *Jeffrey A. Fessler*[⋆]

[⋆]University of Michigan, Department of EECS, Ann Arbor, MI 48109, USA
[†]University of Michigan, Functional MRI Laboratory, Ann Arbor, MI 48109, USA

ABSTRACT

Fast and accurate quantification of spin-spin relaxation parameter T_2 is of importance for clinical MRI applications. Classical spin echo (SE) sequences yield straightforward T_2 estimates, but require undesirably long scans. By contrast, steady-state sequences such as the Dual-Echo Steady-State (DESS) sequence are considerably faster, but produce signals that depend on more complex functions of both desired and nuisance parameters. Conventional method-of-moments estimators exhibit systematic error because of the approximations used to bypass nuisance parameter estimation. To improve T_2 mapping accuracy, we propose a novel, model-based approach to this nonlinear estimation problem. We use a fast scan to estimate nuisance parameters M_0^* and T_1, and then use the exact DESS signal model for regularized T_2 estimation from DESS data, with minimal approximations. MR brain simulation results show that the proposed approach substantially improves T_2 estimation accuracy and precision, compared to conventional method-of-moments estimators.

Index Terms— magnetic resonance imaging, T_2 relaxometry, regularization, signal modeling, MAP estimation

1. INTRODUCTION

Rapid, accurate quantification of relaxation parameters has been of interest in the MRI community for many years. In particular, spin-spin relaxation parameter T_2 shows promise as a potential biomarker for subtle changes in pathology [1], and may be useful for monitoring the progression of poorly-understood neurological and/or autoimmune disorders, such as Parkinson's disease, epilepsy, or multiple sclerosis.

Classical single-echo spin echo sequences yield simple methods for accurately estimating T_2, but require multiple scans at variable echo times, leading to undesirably lengthy acquisitions. Multi-echo SE sequences [2] can eliminate the multiple-scan requirement, but are prone to systematic error in T_2 estimation, due to stimulated-echo contributions that can arise due to transmit field B_1 inhomogeneities [3].

Steady state free precession (SSFP) pulse sequences [4, 5] are, by contrast, considerably faster than spin-echo sequences due to a short repetition time T_R. SSFP techniques are particularly well-suited for relaxometry because the observed signals are highly sensitive to T_1 and T_2 variation. However, short T_R times also cause these signals to be complex functions of both desired and nuisance parameters, thereby complicating quantification. Furthermore, some such methods [6] still require scan repetition at multiple nutation angles, though individual scans are now considerably shorter.

The Dual-Echo Steady-State (DESS) sequence [7] was recently proposed as a promising SSFP imaging technique for T_2 estimation [8]. Since it contains two readouts per excitation, the DESS sequence can be used to reduce scan repetition requirements by collecting twice as much data per scan. As with other SSFP methods, the resulting signals are complex functions of T_1, T_2, and other parameters [9, 10]. To reduce unwanted dependencies, conventional approaches [3, 8] observe that in the large nutation-angle limit, the ratio between the second (SSFP-Echo, S^-) and first (SSFP-FID, S^+) signals is independent of T_1, yielding a simple method-of-moments T_2 estimator. Unfortunately, the low SNR at this limit requires usage of lower nutation angles in practice, thereby introducing bias into the T_2 estimate.

In this work, we mitigate this bias by approaching the T_2 estimation problem through a model-based framework. This method also avoids noise amplification issues inherent to signal division. We first jointly estimate T_2^*-compensated proton density M_0^* and spin-lattice relaxation parameter T_1 maps through regularized reconstruction of DESPOT1 data from as few as two nutation angles [11, 12]. We then iteratively reconstruct T_2 maps using these nuisance parameter estimates and an initialization with the conventional DESS estimate, encouraging piecewise-smoothness through edge-preserving regularization. The resultant T_2 maps maintain significant improvements in both mapping accuracy and precision, over a wide range of nutation angles and repetition times.

2. PROBLEM FORMULATION

2.1. Signal Model

Assuming the DESS crusher [8] dominates any through-voxel field inhomogeneity gradients, one can show from the Bloch equations [13] that steady-state signals immediately prior

Supported in part by NIH grant P01 CA87634. Electronic-mail contact at {gnataraj,jfnielse,fessler}@umich.edu.

(S^-) and following (S^+) the kth excitation can be written as:

$$S^-(kT_R) = -iM_0 \tan\frac{\alpha}{2}\left[1 - \sqrt{\frac{1-E_2^2(T_R)}{1-E_2^2(T_R)/v_1^2}}\right]; \quad (1)$$

$$S^+(kT_R) = iM_0 \tan\frac{\alpha}{2}\left[1 - \frac{1}{v_1}\sqrt{\frac{1-E_2^2(T_R)}{1-E_2^2(T_R)/v_1^2}}\right], \quad (2)$$

where α denotes nutation angle, $E_m(t) := \exp\{-t/T_m\}$, and all T_1 dependency is summarized in the auxiliary variable

$$v_1 := \frac{1 - E_1(T_R)\cos\alpha}{E_1(T_R) - \cos\alpha}. \quad (3)$$

In steady-state imaging, echo time T_E is often on the order of T_R, requiring additional modeling of signal dynamics before and after RF excitation. We account for T_2 relaxation and also model each voxel's macroscopic broadening distribution to be Cauchy($\Delta\bar{\omega}, R_2'$), where $\Delta\bar{\omega}$ denotes the median off-resonance frequency and R_2' is the broadening bandwidth. If we reasonably assume $\Delta\bar{\omega} \approx 0$ for short readouts, and we adopt the usual convention that the signals are symmetrically centered at echo-time T_E before and after the kth excitation,

$$\begin{aligned} S^-(kT_R - T_E) &\approx S^-(kT_R)E_2^{-1}(T_E)e^{-R_2'T_E}; \\ S^+(kT_R + T_E) &\approx S^+(kT_R)E_2(T_E)e^{-R_2'T_E}. \end{aligned} \quad (4)$$

In this work, we seek to accurately estimate T_2 maps from DESS data modeled as (4), but observe that nuisance parameters M_0, T_1, and R_2' complicate this goal. While other user-specified parameters (T_R, T_E, α) are known, these nuisance parameters are unknown, and thus must also be estimated.

2.2. Conventional Method-of-Moments T_2 Estimation

Conventional methods [6, 8] note that for either the large nutation angle limit $\alpha \to \frac{\pi}{2}$ or the long spin-lattice relaxation limit $T_1 \to \infty$, the ratio between these signals approaches a simple model, independent of all other unknowns:

$$\left|\frac{S^-(kT_R - T_E)}{S^+(kT_R + T_E)}\right| \to E_2^2(T_R - T_E), \quad (5)$$

from which T_2 can be easily estimated. This method-of-moments estimator is prone to several sources of error. First, the signal division will amplify noise. Next, because large nutation angles induce low-SNR signals, they are replaced with lower angles in practice. At typical nutation angle choices, the signal ratio deviates from (5) through substantial T_1 dependence, inducing systematic error in the T_2 estimate. Even if DESS data is collected at multiple angles, corresponding total least-squares (TLS) estimates [14] will still suffer from this systematic, T_1-dependent bias. Accordingly, we exclusively consider a TLS-enhanced version of the method-of-moments estimator, henceforth referred to as the TLS estimator.

2.3. A Penalized-Likelihood Estimator

We propose to mitigate T_1-related bias by first estimating unknown nuisance parameters from a fast, separate scan, before performing T_2 estimation. We observe that T_1 and

$$M_0^* := M_0 E_2(T_E)\exp\{-R_2'T_E\} \quad (6)$$

can, for example, be initially estimated from fast Spoiled Gradient-Recalled Echo (SPGR) scans, repeated over as few as two flip angles [6]. We select T_E and T_R to be the same for all SPGR and DESS scans. We estimate M_0^* and T_1 nuisance parameter maps from the SPGR signal model [11],

$$S_{\mathrm{SPGR}} = \frac{M_0^* \sin\alpha(1 - E_1(T_R))}{1 - E_1(T_R)\cos\alpha}, \quad (7)$$

and take these estimates as fixed during the subsequent T_2 estimation. We hereafter focus on estimating T_2 from (4).

We estimate $\mathbf{x} \in \mathbb{R}^N$, with j indexing a total of N voxels and jth element $x_j := \exp\{-T_R/T_{2,j}\}$. We define noisy measurement vectors $\mathbf{y}_l^- := [y_{l,1}^-, \ldots, y_{l,N}^-]^{\mathrm{T}}$ and $\mathbf{y}_l^+ := [y_{l,1}^+, \ldots, y_{l,N}^+]^{\mathrm{T}}$, where l indexes a total of L nutation angles; $\epsilon_{l,j}^{\pm} \sim \mathbb{C}\mathcal{N}(0, \sigma^2)$ is complex, white Gaussian noise; and

$$y_{l,j}^{\pm} := S^{\pm}(kT_R \pm T_E; T_{2,j}, \alpha_l) + \epsilon_{l,j}^{\pm}. \quad (8)$$

$\mathcal{X} := [E_{2,\min}, E_{2,\max}] \subset (0, 1]$ is a solution space corresponding to a range $[T_{2,\min}, T_{2,\max}]$ over which we seek accurate estimation. An ML estimator for $\mathbf{x}$ is then given by:

$$\hat{\mathbf{x}} = \arg\min_{\mathbf{x}\in\mathcal{X}} \Psi_{\mathrm{ML}}(\mathbf{x}), \text{where} \quad (9)$$

$$\Psi_{\mathrm{ML}}(\mathbf{x}) = \frac{1}{2}\sum_{l=1}^{L}\left[||\mathbf{y}_l^- - \mathbf{f}_l^-(\mathbf{x})||^2 + ||\mathbf{y}_l^+ - \mathbf{f}_l^+(\mathbf{x})||^2\right].$$

Observe that the vector functions $\mathbf{f}_l^{\pm}(\mathbf{x})$ are voxel-wise independent mappings from $\mathbb{R}^N \to \mathbb{R}^N$ that naturally extend the corresponding scalar functions $f_l^{\pm}(x) : \mathbb{R} \to \mathbb{R}$, defined as:

$$f_l^-(x) = -iM_0^* \tan\frac{\alpha_l}{2} x^{-\frac{2T_E}{T_R}}\left[1 - \sqrt{\frac{1-x^2}{1-x^2/v_{1,l}^2}}\right]; \quad (10)$$

$$f_l^+(x) = iM_0^* \tan\frac{\alpha_l}{2}\left[1 - \frac{1}{v_{1,l}}\sqrt{\frac{1-x^2}{1-x^2/v_{1,l}^2}}\right]. \quad (11)$$

In addition to the data, we assume prior knowledge that T_2 maps tend to be piecewise-smooth; that is, adjacent voxels are likely to contain similar tissue types, and are thus likely to have similar T_2 values. We thus extend the ML cost function to include an edge-preserving roughness penalty:

$$\Psi_{\mathrm{MAP}}(\mathbf{x}) = \Psi_{\mathrm{ML}}(\mathbf{x}) + \beta R(\mathbf{x}), \quad (12)$$

where $R(\mathbf{x}) = \sum_{k=1}^{K}\phi_k([\mathbf{C}\mathbf{x}]_k)$; $\mathbf{C}$ is a 2D or 3D spatial finite differencing matrix; ϕ_k is a convex, edge-preserving

potential function; k indexes a total K differencing operations; and β is a regularization parameter that controls the level to which roughness in $\mathbf{x}$ is penalized. We then obtain a penalized-likelihood estimate of $\mathbf{x}$ by solving the (non-convex) constrained optimization problem:

$$\hat{\mathbf{x}} = \arg\min_{\mathbf{x}\in\mathcal{X}} \Psi_{\text{MAP}}(\mathbf{x})\,. \tag{13}$$

3. MINIMIZATION TECHNIQUES

Since solution set $\mathcal{X}$ is closed and convex, a preconditioned gradient projection method (PGPM) of the form

$$\mathbf{x}^{(n+1)} = \mathcal{P}_{\mathcal{X}}\left\{\mathbf{x}^{(n)} - \mathbf{D}^{-1}\nabla\Psi_{\text{MAP}}(\mathbf{x}^{(n)})\right\} \tag{14}$$

will monotonically decrease Ψ_{MAP} to a local minimum, as long as preconditioner $\mathbf{D}$ is selected such that $\forall\,\mathbf{x}\in\mathcal{X}$,

$$\nabla^2\Psi_{\text{MAP}}(\mathbf{x}^{(n)}) = \nabla^2\Psi_{\text{ML}}(\mathbf{x}^{(n)}) + \beta\nabla^2 R(\mathbf{x}^{(n)}) \preceq \mathbf{D}\,. \tag{15}$$

Here we have denoted $\mathcal{P}_{\mathcal{X}}\{\cdot\}$ as a projection operator onto $\mathcal{X}$. Observe that because functions $\mathbf{f}_l^{\pm}(\mathbf{x})$ are voxel-wise independent, the Hessian of the ML cost, $\nabla^2\Psi_{\text{ML}}(\mathbf{x}) =$

$$\frac{1}{2}\sum_{l=1}^{L}\left[\nabla^2||\mathbf{y}_l^- - \mathbf{f}_l^-(\mathbf{x})||^2 + \nabla^2||\mathbf{y}_l^+ - \mathbf{f}_l^+(\mathbf{x})||^2\right], \tag{16}$$

is $N\times N$ diagonal. This allows us to first consider bounding the corresponding single-voxel data-fit curvatures $\ddot{\psi}_l^{\pm}(x)$. We then construct $\mathbf{D}$ via a trivial diagonal matrix extension.

We have shown that curvatures $\ddot{\psi}_l^{\pm}(x)$ are convex over $x\in\mathcal{X}, \forall\alpha\in[0,\frac{\pi}{2}]$ and $T_1\in[0,\infty)$. We can therefore bound the curvatures by evaluating at the endpoints of the solution set. In practice, since $\lim_{x\to 1}\ddot{\psi}_l^{\pm}(x)$ can be unbounded, we select $T_{2,\max} < \infty$ (and thus $E_{2,\max} < 1$) to ensure that the endpoint curvatures are finite. With these restrictions, each of the data fidelity terms' curvatures can thereby be bounded as

$$d_l^{\pm} = \max_{x\in\{E_{2,\min},E_{2,\max}\}}\left\{\ddot{\psi}_l^{\pm}(x)\right\}. \tag{17}$$

After computing such bounds $d_{l,j}^{\pm}$ at each voxel $j = 1,\ldots,N$, the corresponding diagonal preconditioner

$$\mathbf{D} = \sum_{l=1}^{L}\text{diag}_j\left\{d_{l,j}^+ + d_{l,j}^-\right\} + \beta\,\text{maxeig}\left\{\nabla^2 R\right\}\mathbf{I}_N \tag{18}$$

ensures that PGPM will monotonically decrease Ψ_{MAP} to a local minimum. The rate of this convergence can be increased at the expense of a tighter solution set $\mathcal{X}$.

We observe in Fig. 1 that even with a restrictive choice of $\mathcal{X}$, selection of $d_l^{\pm}$ via (17) yields a loose bound on the curvature. Quadratic majorizers thus have high curvatures, leading to slow convergence rates of majorize-minimize algorithms [15]. To accelerate convergence, we consider addition of Nesterov's momentum [16] to the PGPM algorithm. The original

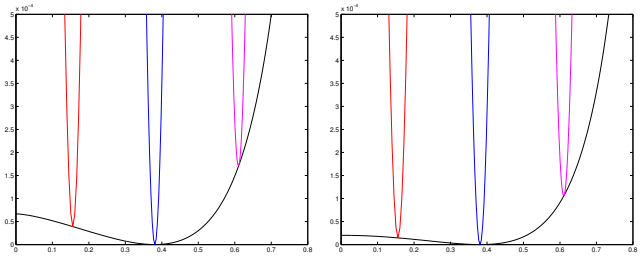

(a) $|y_l^- - f_l^-(x)|^2$ vs. x (b) $|y_l^+ - f_l^+(x)|^2$ vs. x

Fig. 1. Comparisons of a single-voxel data-fit term (black) with quadratic majorizers (colored), whose curvatures are given by (17). High majorizer curvatures cause for slow PGPM convergence without acceleration. Figures created with $\alpha = \frac{\pi}{4}$, $T_R = 20$ms, $T_E = 5$ms, $T_1 = 1000$ms, and $\mathcal{X}$ corresponding to $T_2 = [5, 200]$ms.

algorithm is extended in a straightforward manner to our case of a diagonal preconditioner [17], yielding a simple iteration:

$$\begin{aligned} t_{n+1} &= \left(1+\sqrt{1+4t_n^2}\right)/2 \\ \mathbf{x}^{(n+1)} &= \mathcal{P}_{\mathcal{X}}\left\{\mathbf{z}^{(n)} - \mathbf{D}^{-1}\nabla\Psi_{\text{MAP}}(\mathbf{z}^{(n)})\right\} \\ \mathbf{z}^{(n+1)} &= \mathbf{x}^{(n+1)} + \frac{t_n-1}{t_{n+1}}\left(\mathbf{x}^{(n+1)} - \mathbf{x}^{(n)}\right), \end{aligned} \tag{19}$$

where $\mathbf{z}^{(0)} = \mathbf{x}^{(0)}$ and $t_0 = 1$. This momentum extension to PGPM considerably accelerates convergence, with a marginal increase in storage requirement and computation.

4. EXPERIMENTATION

4.1. Simulated Methods

We combine true M_0, T_1, T_2, and T_2^* maps from the 95th slice of the BrainWeb digital phantom [18] to compute uncorrupted DESS data at 217×181 resolution, using Eq. (4). We corrupt the true data with complex, white Gaussian noise, to yield 40dB SNR raw data. We strive to recover accurate T_2 maps from this raw data, with no prior knowledge of M_0, T_1, or T_2^*.

To estimate the nuisance parameters, we simulate 60dB SPGR data using (7), at "ideal" [6] nutation angles $\alpha = 5, 30^\circ$. From this data, we initially estimate M_0^* and T_1 maps through regularized reconstruction [11]. These estimates are taken to be fixed parameters during subsequent T_2 estimation.

We compute a TLS T_2 estimate [8] from noisy DESS data generated at $\alpha = 45^\circ$. We initialize the proposed method (19) with a median-filtered TLS estimate and iterate until convergence criterion $||\mathbf{x}^{(n)} - \mathbf{x}^{(n-1)}|| < 10^{-6}||\mathbf{x}^{(n)}||$ is satisfied. We choose ϕ_k to be a hyperbolic potential function. We select $\beta = 2^7$ heuristically, though automatic selection methods [19] can be applied in practice. On a 3.5GHz desktop with 32GB RAM, with solution set $\mathcal{X}$ corresponding to a T_2 range of [5,1000]ms, reconstructions take roughly 50s and 35s per slice for SPGR and DESS reconstructions, respectively.

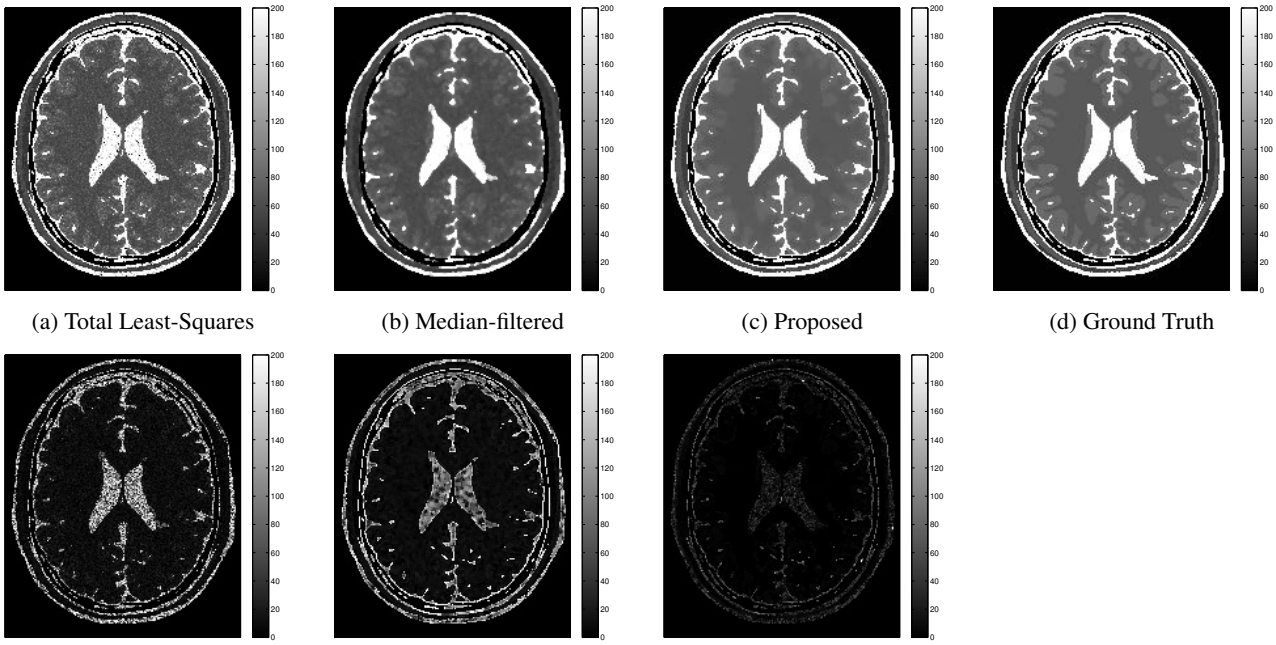

(a) Total Least-Squares (b) Median-filtered (c) Proposed (d) Ground Truth

(e) RMSE = (16.9, 12.3)ms (f) RMSE = (14.1, 10.2)ms (g) RMSE = (4.3, 2.6)ms

Fig. 2. T_2 maps (a, b, c) and corresponding absolute-difference images (e, f, g), with respect to the ground truth (d). Total least squares (a) and median-filtered (b) images reconstructed from 40dB SNR DESS data at RMSE-minimizing flip angle combination $\alpha = 45, 65, 85^\circ$. Proposed image (c) reconstructed from 40dB SNR DESS data at $\alpha = 45^\circ$, following joint estimation of M_0^* and T_1 maps from 60dB SNR SPGR data at $\alpha = 5, 30^\circ$. Tissue-specific errors are spatially averaged over (GM, WM) voxels of interest, and are reported in RMSE.

Tissue	TLS	Median-Filt.	Proposed	Truth
GM	75.1 ± 15.0	73.5 ± 9.6	82.3 ± 4.2	83.0 ± 0.0
WM	60.5 ± 8.0	60.6 ± 3.7	71.0 ± 2.5	70.0 ± 0.0

Table 1. T_2 estimates and standard deviations, spatially averaged over GM and WM regions of interest. Scan protocols match those in Fig. 2. All values reported in (ms). The proposed method exhibits increases in both accuracy and precision over TLS estimates.

4.2. Results and Discussion

Fig. 2 compares the proposed approach against conventional estimates, both before and after median filtering. To ensure a fair comparison in terms of scan time, the conventional estimates are computed from DESS data collected at three nutation angles. These angles, $\alpha = 45, 65, 85^\circ$, are selected to minimize root mean-squared error (RMSE) in the grey-matter (GM) and white-matter (WM) regions of interest.

As evidenced by absolute difference images with respect to the true T_2 map, the TLS estimate is prone to noise amplification due to signal division. Median-filtering reduces noise to some extent, but resulting T_2 maps remain prone to systematic error due to the aforementioned model-mismatch.

Table 1 quantitatively highlights that the proposed method achieves increases in both accuracy and precision over TLS estimates (with or without naïve filtering), particularly in GM and WM regions of interest. Accuracy improvements are due to reduced T_1 induced bias. Precision improvements are due to (1) omission of noise-amplifying signal division, and (2) usage of edge-preserving regularization to encourage piecewise-smooth T_2 estimates. Accuracy and precision increases combine to significantly reduce RMSE values, given in Fig. 2. Such improvements are sustained over a wide range of scan parameters and noise thresholds (results not shown).

5. CONCLUSIONS AND FUTURE WORK

We have presented a novel, model-based approach for T_2 relaxometry from DESS sequences. Compared to conventional methods, we observe that the proposed method improves estimation *accuracy*, primarily due to a reduction of T_1-induced bias through preliminary M_0^*, T_1 joint estimation from SPGR data. We also observe improvements in estimation *precision* through omission of noise-amplifying signal division and utilization of edge-preserving regularization.

Residual errors in the proposed T_2 estimates are likely dominated by the propagation of M_0^*, T_1 estimation error. To bypass this error propagation, it is of future interest to recast the M_0^*, T_1, T_2 estimation problem as a single joint optimization. Such problem reformulation may permit acquisition of fewer scans, yet retain (and possibly improve) the accuracy and precision gains presented in this work.

6. REFERENCES

[1] H-L. M. Cheng, N. Stikov, N. R. Ghugre, and G. A. Wright, "Practical medical applications of quantitative MR relaxometry," *J. Mag. Res. Im.*, vol. 36, no. 4, pp. 805–24, Oct. 2012.

[2] D. Kumar, T. D. Nguyen, S. A. Gauthier, and A. Raj, "Bayesian algorithm using spatial priors for multiexponential T2 relaxometry from multiecho spin echo MRI," *Mag. Res. Med.*, vol. 68, no. 5, pp. 1536–43, Nov. 2012.

[3] R. Heule, C. Ganter, and O. Bieri, "Rapid estimation of cartilage T2 with reduced T1 sensitivity using double echo steady state imaging," *Mag. Res. Med.*, 2014, In press.

[4] W. S. Hinshaw, "Image formation by nuclear magnetic resonance: The sensitive point method," *J. Appl. Phys.*, vol. 47, pp. 3709, 1976.

[5] K. Scheffler, "A pictorial description of steady-states in rapid magnetic resonance imaging," *Concepts in Magnetic Resonance*, vol. 11, no. 5, pp. 291–304, 1999.

[6] S. C. L. Deoni, B. K. Rutt, and T. M. Peters, "Rapid combined T1 and T2 mapping using gradient recalled acquisition in the steady state," *Mag. Res. Med.*, vol. 49, no. 3, pp. 515–26, Mar. 2003.

[7] H. Bruder, H. Fischer, R. Graumann, and M. Deimling, "A new steady-state imaging sequence for simultaneous acquisition of two MR images with clearly different contrasts," *Mag. Res. Med.*, vol. 7, no. 1, pp. 35–42, May 1988.

[8] G. H. Welsch, K. Scheffler, T. C. Mamisch, T. Hughes, S. Millington, M. Deimling, and S. Trattnig, "Rapid estimation of cartilage T2 based on double echo at steady state (DESS) with 3 Tesla," *Mag. Res. Med.*, vol. 62, no. 2, pp. 544–9, Aug. 2009.

[9] M. L. Gyngell, "The steady-state signals in short-repetition-time sequences," *J. Mag. Res.*, vol. 81, no. 3, pp. 474–83, Feb. 1989.

[10] W. Hänicke and H. U. Vogel, "An analytical solution for the SSFP signal in MRI," *Mag. Res. Med.*, vol. 49, no. 4, pp. 771–5, Apr. 2003.

[11] G. Nataraj, J-F. Nielsen, and J. A. Fessler, "Regularized, joint estimation of T1 and M0 maps," in *Proc. Intl. Soc. Mag. Res. Med.*, 2014, p. 3128.

[12] H. Wang and Y. Cao, "Spatially regularized T1 estimation from variable flip angles MRI," *Med. Phys.*, vol. 39, no. 7, pp. 4139–48, 2012.

[13] F. Bloch, "Nuclear induction," *Phys. Rev.*, vol. 70, no. 7-8, pp. 460–74, Oct. 1946.

[14] G. H. Golub and C. F. Van Loan, "An analysis of the total least squares problem," *SIAM J. Numer. Anal.*, vol. 17, no. 6, pp. 883–93, Dec. 1980.

[15] H. Erdoğan and J. A. Fessler, "Monotonic algorithms for transmission tomography," *IEEE Trans. Med. Imag.*, vol. 18, no. 9, pp. 801–14, Sept. 1999.

[16] Y. Nesterov, "A method for unconstrained convex minimization problem with the rate of convergence $O(1/k^2)$," *Dokl. Akad. Nauk. USSR*, vol. 269, no. 3, pp. 543–7, 1983.

[17] D. Kim, S. Ramani, and J. A. Fessler, "Accelerating X-ray CT ordered subsets image reconstruction with Nesterov's first-order methods," in *Proc. Intl. Mtg. on Fully 3D Image Recon. in Rad. and Nuc. Med*, 2013, pp. 22–5.

[18] C. A. Cocosco, V. Kollokian, R. K-S. Kwan, and A. C. Evans, "BrainWeb: Online interface to a 3D MRI simulated brain database," in *Proc. 3rd Intl. Conf. on Functional Mapping of the Human Brain*, 1997, p. S425, NeuroImage, vol. 5 (4, part2/4), May.

[19] S. Ramani, Z. Liu, J. Rosen, J-F. Nielsen, and J. A. Fessler, "Regularization parameter selection for nonlinear iterative image restoration and MRI reconstruction using GCV and SURE-based methods," *IEEE Trans. Im. Proc.*, vol. 21, no. 8, pp. 3659–72, Aug. 2012.